Dilution-induced gel-sol-gel-sol transitions by competitive supramolecular pathways in water

Su, L.; Mosquera, J.; Mabesoone, M.F.J.; Schoenmakers, S.M.C.; Muller, C.; Vleugels, M.E.J.; ... ; Meijer, E.W.

CHEMISTRY

Dilution-induced gel-sol-gel-sol transitions by competitive supramolecular pathways in water

Lu Su[1,2]†, Jesús Mosquera[1,3]†, Mathijs F. J. Mabesoone[1], Sandra M. C. Schoenmakers[1], Cyprien Muller[1], Marle E. J. Vleugels[1], Shikha Dhiman[1], Stefan Wijker[1], Anja R. A. Palmans[1], E. W. Meijer[1,4]*

Fascinating properties are displayed by synthetic multicomponent supramolecular systems that comprise a manifold of competitive interactions, thereby mimicking natural processes. We present the integration of two reentrant phase transitions based on an unexpected dilution-induced assembly process using supramolecular polymers and surfactants. The co-assembly of the water-soluble benzene-1,3,5-tricarboxamide (BTA-EG₄) and a surfactant at a specific ratio yielded small-sized aggregates. These interactions were modeled using the competition between self-sorting and co-assembly of both components. The small-sized aggregates were transformed into supramolecular polymer networks by a twofold dilution in water without changing their ratio. Kinetic experiments show the in situ growth of micrometer-long fibers in the dilution process. We were able to create systems that undergo fully reversible hydrogel-solution-hydrogel-solution transitions upon dilution by introducing another orthogonal interaction.

T he design of interactive and adaptive soft materials requires a complex composition of chemical components for which nature is often a source of inspiration (1). Multicomponent systems formed by multiple associative and dissociative interactions are key signatures of biological matter, but the competitive interplay of all these interactions makes the understanding of certain natural processes difficult (2, 3). Synthetic systems, because of their simplicity, can unravel some of these challenges while yielding new functionalities (4–7). Although this field is still in its infancy, several examples have highlighted its potential for applications in catalysis, electronics, and medicine (8–11), with the development of the lipid nanoparticle–encapsulated mRNA vaccine as an obvious successful highlight in this respect (12).

Liquid-liquid phase separations are often accompanied by the occurrence of reentrant phase transitions (RPTs), which cause fascinating phenomena in these multicomponent systems. Here, changes in temperature and/or addition of one of the components give rise to a recurrence of the original phase (11, 13, 14). This phenomenon was recently found to play a critical role in the formation of intracellular membraneless organelles, which are mainly systems based on liquid-liquid phase separation (15–17). A broader perspective on phase transitions in molecular systems with many components under thermodynamic equilibrium has been presented by Jacobs and Frenkel (18). Their statement—that only minor adjustments to the strengths of intermolecular interactions are required to regulate the formation of different domains with specific compositions—is relevant for our current study.

Two frequently used units to construct aqueous synthetic supramolecular systems are surfactants and supramolecular monomers (6, 19–24). Monomer BTA-EG₄ undergoes supramolecular polymerization in water to afford one-dimensional aggregates at micromolar concentration driven by hydrogen bonding and hydrophobic effects, and is made water-soluble by hydrophilic tetraethylene glycol groups (Fig. 1A and fig. S6) (24). Dynamic hydrogels are formed at concentrations above 8 mM (figs. S7 and S8) (25). The cationic surfactant octyltrimethylammonium bromide (OTAB) forms spherical micelles with a hydrodynamic diameter ~2 nm above its critical micelle concentration (CMC = ~297 mM at 20°C) (26). An unexpected finding sparked our attention when studying orthogonality by combining these two units. We observed that the addition of OTAB provoked the full disruption of the BTA-EG₄ hydrogel. Surprisingly, the resulting solution was transformed into a transparent hydrogel upon dilution, followed by reentering the solution phase with further dilution, giving rise to a supramolecular sol-gel-sol RPT in water. The first two states were visualized by cryogenic transmission electron microscopy (cryo-TEM) (Fig. 1B) and small-angle x-ray scattering (SAXS) (fig. S9). This process was fully reversible by increasing the concentration and led us to investigate the underlying mechanism of this hitherto undescribed dilution-induced supramolecular poly-

merization in water. It is combined with the development of two integrated RPTs (gel-sol-gel-sol) upon dilution with the supramolecular units shown in Fig. 1.

To elucidate the pathways that direct the sol-gel transition upon dilution, we investigated the interaction between BTA-EG₄ and a library of surfactants at micromolar concentrations (figs. S10 to S16). We illustrate our detailed explorations using a combination of spectroscopic, cryo-TEM, light scattering, isothermal titration calorimetry, and theoretical techniques (Fig. 2 and figs. S1 to S5, S17 to S21) by taking the cationic surfactant cetrimonium bromide (CTAB, CMC ≈ 1 mM) as an example. Nuclear magnetic resonance (NMR) and cryo-TEM measurements of BTA-EG₄ (250 μM) were performed in the presence of 0, 1, 2, and 3 eq. of CTAB (Fig. 2, A and B). As a result of the formation of micrometer-sized polymers in D₂O, no resonances from BTA-EG₄ were observed in the NMR, whereas the sample containing 250 μM CTAB showed sharp and well-split peaks. CTAB peaks disappeared when mixed in equimolar ratio with BTA-EG₄ in NMR, and cryo-TEM confirmed the presence of micrometer-long aggregates (Fig. 2B). Together, these results indicate that all the surfactants are integrated in the polymers. However, when more equivalents of CTAB were applied, we observed a gradual increase in intensity and resolution of the peaks associated with BTA-EG₄. At 2 eq. of CTAB, the ethylene glycol peak of BTA-EG₄ appeared; ¹H diffusion-ordered spectroscopy (DOSY) NMR (fig. S17) revealed that all the surfactants were still embedded, but in much smaller assemblies. These smaller aggregates were confirmed by cryo-TEM images showing fibers less than 500 nm in length. At 3 eq. of CTAB, both signals corresponding to the short BTA-EG₄/CTAB fibers and BTA-EG₄/CTAB micelles were observed in DOSY NMR; cryo-TEM showed small spherical aggregates and occasionally short fibers. Ultraviolet-visible (UV-vis) spectroscopy confirmed fiber disruption and the formation of small BTA aggregates (Fig. 2C). This transition was dependent on the overall concentration as well as the ratio of both components (Fig. 2D), with more surfactants needed at lower BTA concentrations. The saturation of the polymer with surfactants destabilized the structure and destroyed the fibers at high concentrations of surfactant, most probably as a result of electrostatic and/or geometric constraints in the structures formed (Fig. 2E).

Studies with other surfactants revealed three relevant conclusions: (i) The affinity between the surfactant and BTA-EG₄ is determined by the length of the aliphatic chain of the surfactant, (ii) BTA-EG₄ fibers are unstable below the CMC of the surfactants, and (iii) the transition is dependent on both the overall concentration and the ratio of the components.

[1]Institute for Complex Molecular Systems, Laboratory of Macromolecular and Organic Chemistry, Eindhoven University of Technology, 5600 MB Eindhoven, Netherlands. [2]Leiden Academic Centre for Drug Research, Leiden University, 2333 CC Leiden, Netherlands. [3]Centro de Investigacións Científicas Avanzadas, Universidade da Coruña (CICA), A Coruña, Spain. [4]School of Chemistry and RNA Institute, University of New South Wales, Sydney, NSW 2052, Australia.
*Corresponding author. Email: e.w.meijer@tue.nl
†These authors contributed equally to this work.
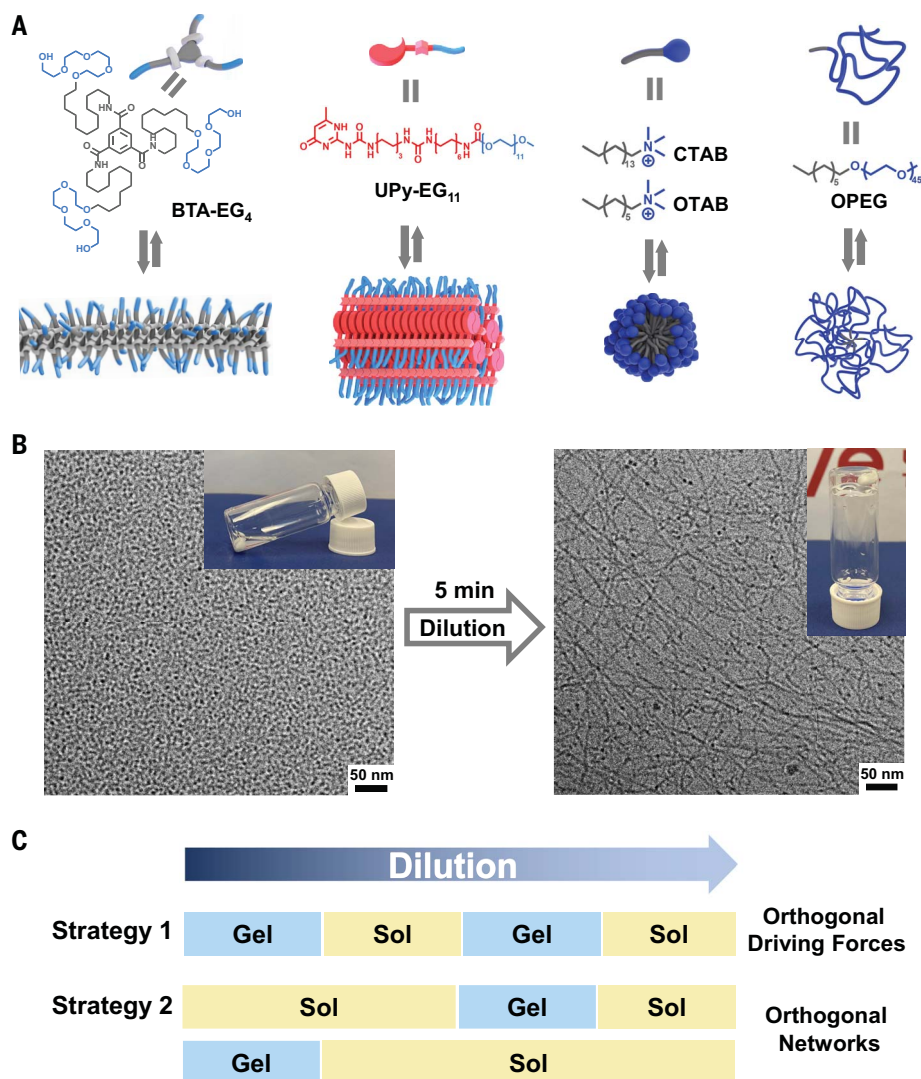
Fig. 1. Dilution-induced gelation in water. (**A**) Supramolecular components and their individual assemblies in water. (**B**) Cryo-TEM images of dilution-induced gelation in a **BTA-EG₄**/OTAB system. Left: A solution of **BTA-EG₄** (4 wt %, 31 mM) and OTAB (6.5 eq., 202 mM) shows small aggregates with a diameter of 5 to 8 nm, suggesting the presence of micellar **BTA-EG₄**/OTAB complexes. Right: A transparent hydrogel of **BTA-EG₄** (2 wt %) and OTAB (101 mM), generated upon twofold dilution with MQ-H₂O, shows an entangled **BTA-EG₄** fiber network. Scale bar, 50 nm. (**C**) Two strategies for dilution-induced gel-sol-gel-sol transitions by competitive supramolecular pathways in water.

From these results, we hypothesize that the sol-gel transition upon dilution is driven by the concentration-dependent complexation of surfactants to **BTA-EG₄** polymers. To corroborate this hypothesis, we constructed a thermodynamic mass-balance model that describes competition among supramolecular polymerization, micellization, complexation of CTAB to the polymers, and polymer collapse (Fig. 2, E and F, figs. S1 to S5, and supplementary text). We subsequently studied the dilution-induced effect of a solution of **BTA-EG₄** with 3 eq. of CTAB, in which only small aggregates exist. Upon dilution, peaks corresponding to both **BTA-EG₄** and CTAB gradually broadened and weakened in NMR (Fig. 2G) while the

characteristic peaks (211 and 227 nm) in UV-vis spectra related to fiber structure appeared (Fig. 2H), as corroborated by cryo-TEM (fig. S21). We hypothesize that CTAB is released when the overall concentration decreases, thereby enabling the elongation of the BTA fiber to eventually achieve micrometer-long structures. The dilution-induced supramolecular polymerization became faster upon adding more water (fig. S20).

With an understanding of the mechanisms underlying the dilution-induced supramolecular polymerization in water, an integration of two RPTs was developed by introducing an additional orthogonal interaction through two different strategies (Fig. 1C). The first strategy

uses the intrinsic property of a polymeric surfactant to lead to further aggregation at higher concentration, whereas the second strategy takes advantage of an orthogonal supramolecular double network with a different gelation concentration window.

The polymeric surfactant, octyl polyethylene glycol (OPEG, 2 kDa; Fig. 1A and figs. S22 and S23) was synthesized with a C8-spacer. The interaction of OPEG with **BTA-EG₄** at micromolar concentration was evaluated by UV-vis, NMR, and cryo-TEM, showing a behavior similar to that observed for CTAB (figs. S24 and S25). Interestingly, an optimized **BTA-EG₄**: OPEG molar ratio of 2:3 ([**BTA-EG₄**] = 80 mM) in Milli-Q (MQ)–H₂O gave rise to an opaque **Gel 1** with a mesh size of ~10 to 20 nm as indicated by cryo-TEM (Fig. 3A) and SAXS (fig. S36). The densely packed network was composed of wormlike fibers of fused **BTA-EG₄**/OPEG micelles. Rheological experiments showed a storage modulus, G', of up to 2 kPa with a complex viscosity, η^*, above 2 kPa·s, as well as a fast and near-complete self-healing behavior (Fig. 3, C to E). When diluting this gel with water to [**BTA-EG₄**] = 35 mM, a solution was obtained after equilibrium, owing to the dissociation of the fused micelles as depicted by cryo-TEM and SAXS. In line with the morphology transition, η^* dropped to ~1 Pa·s. When this solution was further diluted to [**BTA-EG₄**] = 27 mM, which is below the CMC of OPEG (~42 mM; fig. S26), a transparent and dynamic **Gel 2** was formed with G' of ~5 Pa and η^* of ~10 Pa·s. This gelation was triggered by the dissociation/release of OPEG from the **BTA-EG₄**/OPEG micellar complex, which enabled the elongation of the BTA fibers and led to the formation of the typical, entangled **BTA-EG₄** fiber network. With further dilution to [**BTA-EG₄**] = 0.8 mM and still the same **BTA-EG₄**: OPEG molar ratio of 2:3, the hydrogel changed into a viscous solution showing η^* of ~0.4 Pa·s and micrometer-long individual fibers. A detailed characterization of this gel-sol-gel-sol system (cryo-TEM, SAXS, and rheology) is presented in figs. S27 to S36.

The good biocompatibility of **BTA-EG₄** [27] provides further opportunity for application of this multicomponent system in more complex media. Phosphate-buffered saline and DMEM/F12 basal medium were used for the whole process, showing RPT behavior identical to that observed in MQ-H₂O (fig. S37). Additionally, when physiological temperature was applied, G' of **Gel 1** became reduced by a factor of 8 (G' ~ 250 Pa), probably owing to a fastened dissociation of **BTA-EG₄**/OPEG micelles (fig. S38).

The second strategy relies on an orthogonal supramolecular network formed by water-soluble supramolecular polymers based on the ureido-pyrimidinone unit (**UPy-EG₁₁**, Fig. 1A), which is less dynamic than **BTA-EG₄** polymers [28].
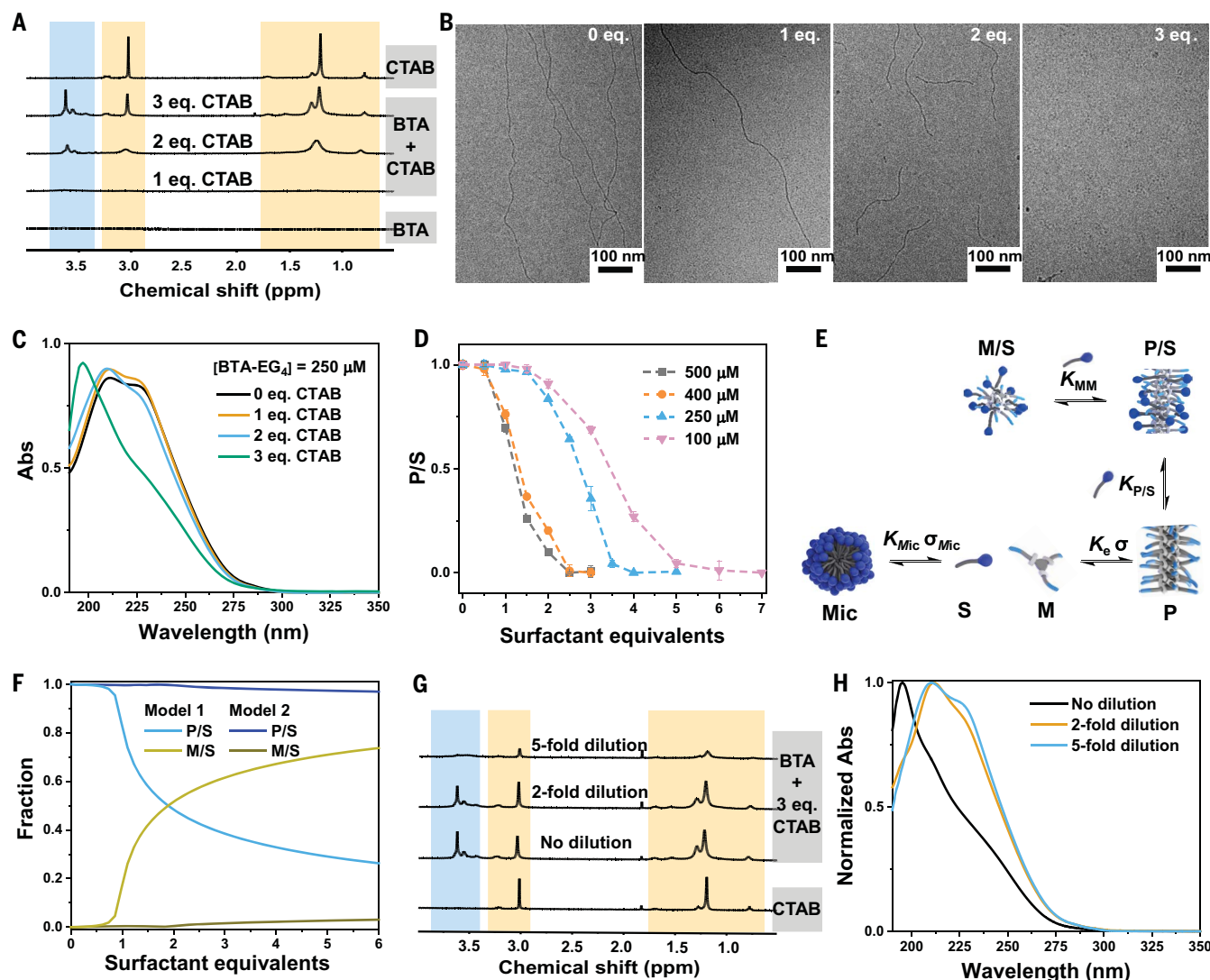
Fig. 2. Interaction and dilution-induced assembly of BTA-EG₄ and CTAB in water. (**A** to **C**) ¹H NMR spectra (400 MHz, D₂O; peaks corresponding to BTA and CTAB are in blue and yellow zones, respectively) (A), cryo-TEM images (scale bar, 100 nm) (B), and UV-vis spectra (C) of **BTA-EG₄** (250 μM) in the presence of 0, 1, 2, and 3 eq. of CTAB, respectively. (**D**) Experimental fraction curves of **BTA-EG₄**/CTAB polymer obtained by normalizing the UV absorbance at 227 nm. The concentration of **BTA-EG₄** was held constant (500, 400, 250, or 100 μM, respectively) while CTAB content was varied. (**E**) Thermodynamic model for the cooperative, competitive pathways, with M, P, S, and Mic representing **BTA-EG₄** monomer, **BTA-EG₄** polymer, free surfactant, and surfactant micelle, respectively, and K_i and σ_i the equilibrium constant and cooperativity parameter of process i. (**F**) Simulated fraction curves of P/S and M/S with 1 eq. (model 1) and 2 eq. (model 2) of [CTAB]/[**BTA-EG₄**] accommodations, in which the concentration of **BTA-EG₄** was held constant (250 μM) while the surfactant content was varied. (**G** and **H**) ¹H NMR spectra (400 MHz, D₂O; peaks corresponding to BTA and CTAB are in blue and yellow zones, respectively) (G) and UV-vis spectra (H) of [**BTA-EG₄**]/[CTAB] (1/3) upon dilution, with [**BTA-EG₄**]ᵢₙᵢₜᵢₐₗ = 250 μM. CTAB absorption in all UV-vis spectra was removed for clarity.

In water, **UPy-EG₁₁** gives rise to micrometer-long bundled fibers with a width of ~5 to 14 nm. **UPy-EG₁₁**/CTAB interactions were confirmed by ¹H NMR (fig. S39). However, **UPy-EG₁₁** and **UPy-EG₁₁**/CTAB mixtures (up to 5 eq. of CTAB) showed almost identical UV spectra and cryo-TEM images, indicating that CTAB binds with **UPy-EG₁₁** bundles yet does not markedly disrupt the supramolecular polymer. When mixed, **BTA-EG₄** and **UPy-EG₁₁** form self-sorted homopolymers. Hence, **BTA-EG₄**, **UPy-EG₁₁**, and a surfactant make an ideal combination to construct an interpenetrating double network

consisting of different gelation windows. As depicted in Fig. 3B, F to H, an opaque hydrogel **Gel 1′** was fabricated with a **BTA-EG₄:UPy-EG₁₁:OTAB** molar ratio of 3.2:1:21.2 at [**BTA-EG₄**] of 93 mM in MQ-H₂O. **Gel 1′** is mainly stabilized by the **UPy-EG₁₁** network, whereas **BTA-EG₄** exists as **BTA-EG₄**/OTAB micelles. Upon dilution to [**BTA-EG₄**] = 46.7 mM, the **UPy-EG₁₁** network was not dense enough to construct a three-dimensional network that tightly held all the water. As the length of the **BTA-EG₄** fibers was not sufficient to form a network because of interaction with the sur-

factant, a transparent solution with a low η* of ~1 Pa·s was accomplished. Further dilution yielded the sol-gel-sol transition as in the first strategy. All results of the detailed characterization are presented in figs. S40 to S43.

After exploring the different states at specific concentrations, we tested methods for tracking the formation of these polymers upon dilution. We used total internal reflection fluorescence microscopy (TIRFM) to trace the in situ formation of the supramolecular polymeric fibers after the addition of droplets of concentrated solution to an aqueous film (Fig. 4).

Fig. 3. Dilution-induced gel-sol-gel-sol transitions in water by using a two-component (BTA-EG$_4$/OPEG) or three-component (BTA-EG$_4$/UPy-EG$_{11}$/OTAB) system, respectively. (**A**) Cryo-TEM images and schematic illustrations of gel-sol-gel-sol transitions of a **BTA-EG$_4$**/OPEG system with their macro-scopic images and molecular-level illus-trations as insets above and below. (**B**) Schematic illustrations of gel-sol-gel-sol transitions of a **BTA-EG$_4$/UPy-EG$_{11}$/** OTAB system, displayed as in (A). (**C** and **F**) Complex viscosity points (ω = 1 rad/s, 1% strain, 20°C) corresponding to the gel-sol-gel-sol transitions in the **BTA-EG$_4$**/OPEG system (C) and the **BTA-EG$_4$/UPy-EG$_{11}$/**OTAB system (F), with the dashed line fitted through the cubic spline curve. (**D** and **G**) Frequency-dependent oscillatory rheology (1% strain, 20°C) of the **BTA-EG$_4$**/OPEG system (D), showing that **Gel 1** ([**BTA-EG$_4$**] = 80 mM) has a stronger network than **Gel 2** ([**BTA-EG$_4$**] = 27 mM), and the **BTA-EG$_4$/UPy-EG$_{11}$/**OTAB sys-tem (G), showing that **Gel 1′** ([**BTA-EG$_4$**] = 93 mM) has a stronger network than **Gel 2′** ([**BTA-EG$_4$**] = 15.5 mM). (**E** and **H**) Step-strain measurements with applied oscillatory strain alternated between 1% and 1000% for 30-s periods (ω = 1 rad/s, 20°C) in **Gel 1** of the **BTA-EG$_4$**/OPEG system (E) and **Gel 1′** of the **BTA-EG$_4$/UPy-EG$_{11}$/** OTAB system (H).
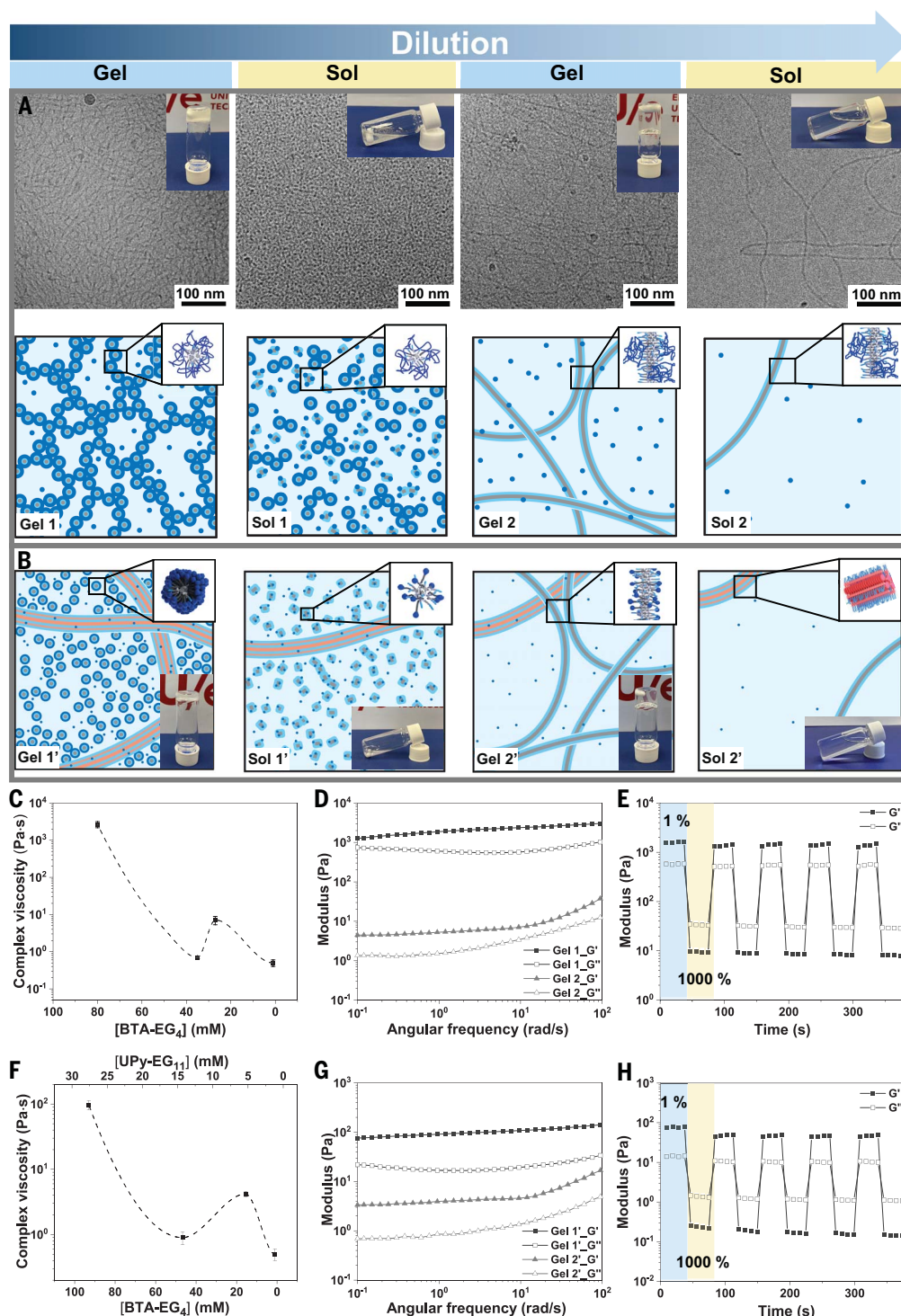
(See figs. S44 to S46 for details of the experi-mental setup.) When an aqueous droplet of [**BTA**]:[**CTAB**] (1:3, [**BTA**] = 250 μM), contain-ing 5% **BTA-Cy3** for visualization, was pipetted into the aqueous film and thus 100-fold diluted in situ, supramolecular fibers started to grow at several positions out of droplets (Fig. 4, A to C). The relatively slow process in thin films enabled us to follow the growth over time. Some of the fibers became many tens of micrometers long (Fig. 4A). In some cases, the fibers were connected to other droplets (Fig. 4C). In other cases, the fibers both grew and shrank, and the pulling of droplets by the contracting fibers could be observed (Fig. 4D and movies S1 to S4). We ascribe the growth and the shrinkage to concentration gradients from the droplet and against the droplet, respectively—a phenomenon similar to the dynamic interconnected networks formed by Marangoni flows in the mesoscale position-ing of amphiphiles when extruded from the droplets (*29*). These results emphasize the crit-ical role of concentrations in multicomponent systems and are useful to understand several phenomena in biology, where RPTs are critically important to understand cellular condensates.
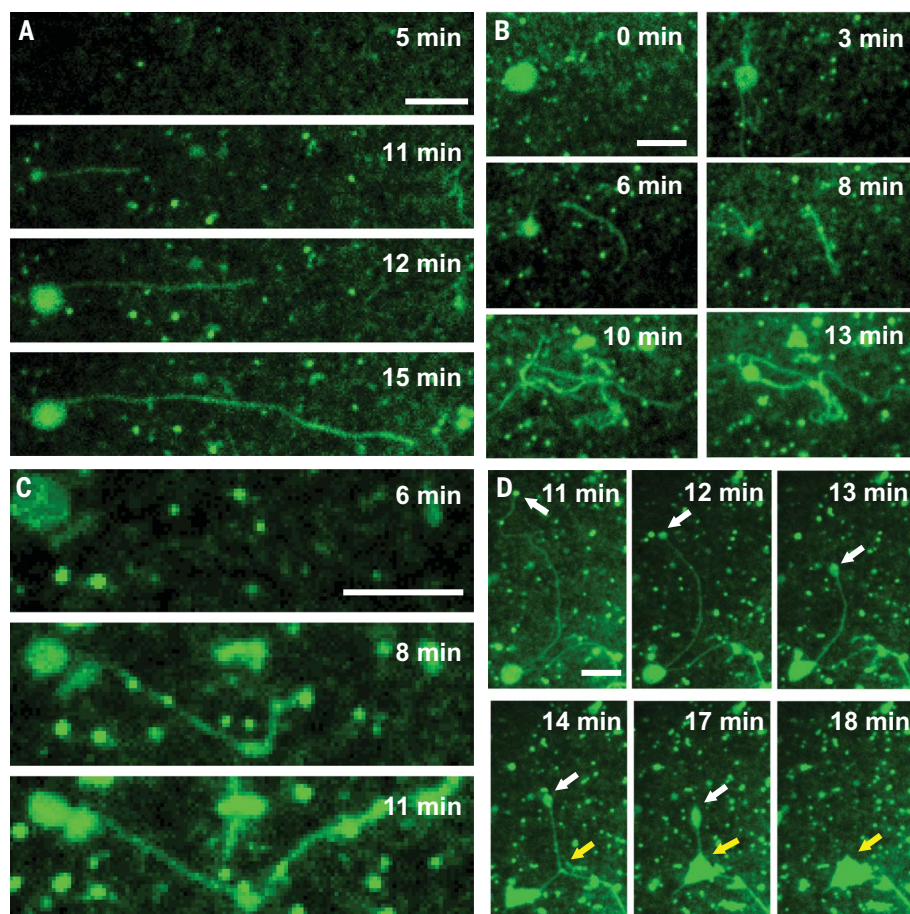
Fig. 4. Kinetic in situ formation of fibers upon dilution. (**A** to **C**) TIRFM images from movies S1 and S2 upon addition of **BTA-EG$_4$**/CTAB droplets to a film of PBS over time. The droplets in time adhere to the surface and fibers are formed after several minutes, using 1% **BTA-biotin**. The green fluorescence is the result of 5% **BTA-Cy3**; the higher the intensity, the higher the concentration of **BTA**. The increase of the droplet size results from an increased adhesion of the droplet to the surface. The increase in length of the fibers is the result of dilution-induced self-assembly/polymerization by diffusion of aggregates from the densely packed droplet to the continuous water film. (**D**) Snapshots from movies S3 and S4 of the shrinkage (white arrow) and connection (yellow arrow) of the fibers due to concentration gradients. Scale bar, 5 μm.

REFERENCES AND NOTES

1. R. Merindol, A. Walther, *Chem. Soc. Rev.* **46**, 5588–5619 (2017).
2. K. Simons, E. Ikonen, *Nature* **387**, 569–572 (1997).
3. W. Baumeister, J. Walz, F. Zühl, E. Seemüller, *Cell* **92**, 367–380 (1998).
4. G. Vantomme, E. W. Meijer, *Science* **363**, 1396–1397 (2019).
5. J.-F. Lutz, J.-M. Lehn, E. W. Meijer, K. Matyjaszewski, *Nat. Rev. Mater.* **1**, 16024 (2016).
6. T. Aida, E. W. Meijer, S. I. Stupp, *Science* **335**, 813–817 (2012).
7. E. Mattia, S. Otto, *Nat. Nanotechnol.* **10**, 111–119 (2015).
8. Q. Wan, W. P. To, X. Chang, C. M. Che, *Chem* **6**, 945–967 (2020).
9. S. Li *et al.*, *J. Am. Chem. Soc.* **140**, 10794–10802 (2018).
10. D. A. Wilson, R. J. M. Nolte, J. C. M. van Hest, *Nat. Chem.* **4**, 268–274 (2012).
11. F. Helmich *et al.*, *Angew. Chem. Int. Ed.* **49**, 3939–3942 (2010).
12. N. Pardi, M. J. Hogan, F. W. Porter, D. Weissman, *Nat. Rev. Drug Discov.* **17**, 261–279 (2018).
13. E. A. Clark, J. E. G. Lipson, *Polymer* **53**, 536–545 (2012).
14. T. M. Hermans *et al.*, *Nat. Nanotechnol.* **4**, 721–726 (2009).
15. P. R. Banerjee, A. N. Milin, M. M. Moosa, P. L. Onuchic, A. A. Deniz, *Angew. Chem. Int. Ed.* **56**, 11354–11359 (2017).
16. J. A. Riback *et al.*, *Nature* **581**, 209–214 (2020).
17. Y. Shin, C. P. Brangwynne, *Science* **357**, eaaf4382 (2017).
18. W. M. Jacobs, D. Frenkel, *Biophys. J.* **112**, 683–691 (2017).
19. R. J. Brea *et al.*, *J. Am. Chem. Soc.* **140**, 17356–17360 (2018).
20. M. P. Hendricks, K. Sato, L. C. Palmer, S. I. Stupp, *Acc. Chem. Res.* **50**, 2440–2448 (2017).
21. J. Kang *et al.*, *Science* **347**, 646–651 (2015).
22. G. González-Rubio *et al.*, *Science* **368**, 1472–1477 (2020).
23. A. Heeres *et al.*, *J. Am. Chem. Soc.* **125**, 14252–14253 (2003).
24. C. M. A. Leenders *et al.*, *Chem. Commun.* **49**, 1963–1965 (2013).
25. E. Vereroudakis *et al.*, *ACS Cent. Sci.* **6**, 1401–1411 (2020).
26. R. Zieliński, *J. Colloid Interface Sci.* **235**, 201–209 (2001).
27. S. Varela-Aramburu *et al.*, *Biomacromolecules* **21**, 4105–4115 (2020).
28. S. I. S. Hendrikse *et al.*, *Chem. Commun.* **53**, 2279–2282 (2017).
29. A. van der Weijden, M. Winkens, S. M. C. Schoenmakers, W. T. S. Huck, P. A. Korevaar, *Nat. Commun.* **11**, 4800 (2020).

Science

Dilution-induced gel-sol-gel-sol transitions by competitive supramolecular pathways in water

Lu SuJesús MosqueraMathijs F. J. MabesooneSandra M. C. SchoenmakersCyprien MullerMarle E. J. VleugelsShikha DhimanStefan WijkerAnja R. A. PalmansE. W. Meijer

Dilution-induced ordering

Many molecules, such as surfactants, can form ordered structures when placed in solution. Typically, the systems become more ordered and the structures change from spheres to elongated shapes as the concentration is increased. Su *et al*. studied a system of benzene-1,3,5-tricarboxamide) (BTA-EG4) with the cationic surfactant octyltrimethylammonium bromide (OTAB), in water (see the Perspective by Webber). BTA-EG4 undergoes supramolecular polymerization in water and will form hydrogels at higher concentrations, whereas OTAB will form small aggregates. However, when combined, the OTAB initially disrupts the BTA-EG4 hydrogels, but these can be reestablished upon dilution because this lessens the effect of the surfactant. With careful engineering, this can be expanded to a gel-sol-gel-sol system as a function of concentration. —MSL

View the article online
https://www.science.org/doi/10.1126/science.abn3438
Permissions
https://www.science.org/help/reprints-and-permissions

Use of this article is subject to the Terms of service